

Estimating topological charge of propagating vortex from single-shot non-imaged speckle

Li Chen (陈丽)¹, Rakesh Kumar Singh^{1,2}, Aristide Dogariu³, Ziyang Chen (陈子阳)^{1,3*}, and Jixiong Pu (蒲继雄)^{1,4**}

¹College of Information Science and Engineering, Huaqiao University, Xiamen 361021, China

²Department of Physics, Indian Institute of Technology (BHU), Varanasi 221005, Uttar Pradesh, India

³CREOL, College of Optics and Photonics, University of Central Florida, Orlando, FL 32816-2700, USA

⁴Fujian Provincial Key Laboratory of Light Propagation and Transformation, Huaqiao University, Xiamen 361021, China

*Corresponding author: ziyang@hqu.edu.cn

**Corresponding author: jixiong@hqu.edu.cn

Received July 21, 2020 | Accepted September 22, 2020 | Posted Online December 10, 2020

Encoding information using the topological charge of vortex beams has been proposed for optical communications. The conservation of the topological charge on propagation and the detection of the topological charge by a receiver are significant in these applications and have been well established in free-space. However, when vortex beams enter a diffuser, the wavefront is distorted, leading to a challenge in the conservation and detection of the topological charge. Here, we present a technique to measure the value of the topological charge of a vortex beam obscured in the randomly scattered light. The results of the numerical simulations and experiments are presented and are in good agreement. In particular, only a single-shot measurement is required to detect the topological charge of vortex beams, indicating that the method is applicable to a dynamic diffuser.

Keywords: intensity correlation; vortex beam; scattering.

DOI: [10.3788/COL202119.022603](https://doi.org/10.3788/COL202119.022603)

1. Introduction

Vortex beams refer to beams with a helical phase structure $\exp(il\phi)$, where l represents the topological charge. Each photon of the vortex beam carries a definite orbital angular momentum (OAM) of $l\hbar$. The OAM of vortex beams has been used to encode information for optical communication, trap particles for optical manipulation, etc.^[1–15]. In these applications, the measurement of the topological charge of vortex beams is necessary. Methods have been proposed to measure topological charges based on interference^[16–19] and diffraction intensity^[20–25]. The interferometric method includes the use of a Mach–Zehnder interferometer^[16], a lateral shear interferometer^[17], and double-slit interference^[18]. The diffraction method includes the use of a triangular aperture^[20], annular gratings^[22], a tilted convex lens (L)^[23], and a translated single slit^[24].

The propagation of light through inhomogeneous media will scramble the wavefront of the light, leading to a speckle pattern. In such a case, coherent noise affects the information content in the imaging system. Recently, single-shot measurement using interferometric spatial heterodyning detection in conjunction with computational image processing has been proposed to suppress the coherent noise, where the imaging quality can be

greatly improved even in conditions of low signal-to-noise ratio^[26]. In the presence of a diffuser, the aforementioned conventional methods to measure the topological charge of the vortex beam are not applicable. The presence of a diffuser in the path of the vortex beam makes speckle patterns have no direct resemblance with vortex beam. Some studies have aimed at retrieving the information of vortex beams from the speckle^[27–30]. These studies are limited to an imaging system^[28,29] or require several measurements^[27,30]. Analyzing the correlation property in Hanbury Brown–Twiss (HBT) interferometry is a widely used method, and it has also been utilized to examine twisted light, based on the idea of an azimuthal analog of the HBT effect^[31], and measure radial and azimuthal mode indices of the vortex beams^[32]. Nevertheless, these experiments are implemented without a diffuser^[31,32].

In this paper, we propose a new method to measure the magnitude of the topological charge of vortex beams from single-shot speckle intensity measurement. This method is realized using spatial statistical optics, wherein the ensemble average is replaced by the spatial average^[33]. The Fourier transform of the intensity correlation, which is estimated by the measured resultant speckle field, provides a method to determine the magnitude of the topological charge of a vortex beam. The basic

principle, the experimental results, and numerical simulations of this technique are described in detail. The experimental results are compared with the numerical simulations for vortex beams with topological charges of 1–3.

2. Theory

Let us consider the two-dimensional (2D) transverse electric field of coherent light. The polarized vector field can be represented by two orthogonal components $E_x(\mathbf{r}_1, t)$ and $E_y(\mathbf{r}_1, t)$, where x and y denote the directions of the polarization components, and \mathbf{r}_1 is the position vector in the transverse plane for a fixed time t . In the source plane, the coherent field can be described as

$$E(\mathbf{r}_1) = \begin{pmatrix} E_x(\mathbf{r}_1) \\ E_y(\mathbf{r}_1) \end{pmatrix}, \quad (1)$$

which is the typical representation of the coherent field in an orthogonal basis $E(\mathbf{r}_1) = \hat{e}_x E_x(\mathbf{r}_1) + \hat{e}_y E_y(\mathbf{r}_1)$, where \hat{e}_x and \hat{e}_y denote the horizontal and vertical polarization states of light, respectively. After propagating through a phase-only screen, both polarization states acquire a random phase $\phi_r(\mathbf{r}_1)$.

This coherent field, with a spatially varying phase, propagates z distance to an observation plane, as illustrated in Fig. 1. In this plane, the field becomes

$$E_m(\mathbf{r}) = \int G(\mathbf{r}, \mathbf{r}_1) E_m(\mathbf{r}_1) e^{i\phi_r(\mathbf{r}_1)} d\mathbf{r}_1, \quad (2)$$

where $m = x, y$, and \mathbf{r} is the transverse spatial coordinate in the observation plane. $G(\mathbf{r}, \mathbf{r}_1)$ is Green's function for free-space propagation:

$$G(\mathbf{r}, \mathbf{r}_1) = \frac{\exp(ikz)}{i\lambda z} \exp\left(ik \frac{|\mathbf{r}_1|^2 - 2\mathbf{r}_1 \cdot \mathbf{r} + |\mathbf{r}|^2}{2z}\right), \quad (3)$$

where λ and $k = 2\pi/\lambda$ are the wavelength and wave number of the light, respectively.

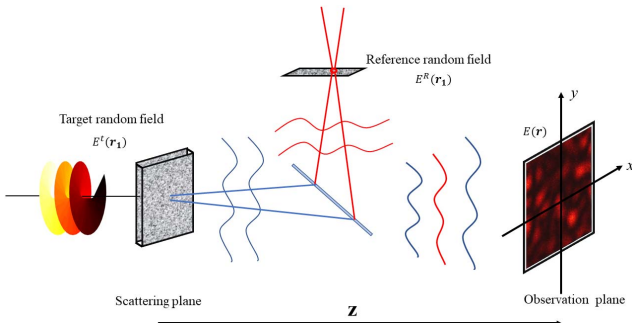


Fig. 1. Geometry of sources, scattering plane, observation plane, and propagation system.

To examine the role of the local state of polarization, we consider that the field is transmitted through a polarizer, oriented at angle θ . The field at the source plane in Eq. (2) is modified to

$$E'_m(\mathbf{r}_1, \theta) = P(\theta) \begin{pmatrix} E_x(\mathbf{r}_1) \\ E_y(\mathbf{r}_1) \end{pmatrix}, \quad (4)$$

where $P(\theta) = \begin{pmatrix} \cos^2 \theta & \sin \theta \cos \theta \\ \sin \theta \cos \theta & \sin^2 \theta \end{pmatrix}$ is the Jones matrix of the linear polarizer, oriented at θ with respect to the horizontal (x) polarization state.

Assuming that, the detected field, given by Eq. (4), is the superposition of two statistically independent spatially varying fields. For example, these fields can be a target t and a reference R component, such that the complex field at the observation plane becomes

$$E'_m(\mathbf{r}, \theta) = E'_m{}^t(\mathbf{r}, \theta) + E'_m{}^R(\mathbf{r}, \theta). \quad (5)$$

In the case where the polarization directions of the target and reference beams are orthogonal, the resultant intensity at the observation plane is

$$I(\mathbf{r}, \theta) = I^t(\mathbf{r}, \theta) + I^R(\mathbf{r}, \theta), \quad (6)$$

where $I^s(\mathbf{r}, \theta) = |E'_x{}^s(\mathbf{r}, \theta)|^2 + |E'_y{}^s(\mathbf{r}, \theta)|^2$ and $s = t, R$ represents the two sources: target or reference. This intensity can be expressed as

$$I^s(\mathbf{r}, \theta) = \cos^2 \theta |E_x^s(\mathbf{r})|^2 + \sin^2 \theta |E_y^s(\mathbf{r})|^2 + \sin \theta \cos \theta [E_x^s(\mathbf{r}) E_y^{s*}(\mathbf{r}) + E_x^{s*}(\mathbf{r}) E_y^s(\mathbf{r})], \quad (7)$$

where $*$ represents the complex conjugate. For different polarizer angles θ and the case without the polarizer, Eq. (7) can be represented in matrix form, as in Eq. (8). In Eq. (8), $I^s(\mathbf{r})$ represents the random intensity pattern without a polarizer, i.e., $P(\theta) = 1$.

The traditional framework of temporal statistical optics is not applicable to the random field described by Eq. (5). Spatial statistics, in which the ensemble average is replaced by the spatial average, permits the analysis of random fields that are frozen in time but spatially varying and is thus suitable for the time frozen random pattern in our case^[33].

$$\begin{aligned}
 & \begin{bmatrix} I^s(\mathbf{r}, 0^\circ) \\ I^s(\mathbf{r}, 45^\circ) \\ I^s(\mathbf{r}, 90^\circ) \\ I^s(\mathbf{r}, -45^\circ) \\ I^s(\mathbf{r}) \end{bmatrix} \\
 &= \begin{bmatrix} |E_x^s(\mathbf{r})|^2 \\ \frac{1}{2}|E_x^s(\mathbf{r})|^2 + \frac{1}{2}[E_x^s(\mathbf{r})E_y^{s*}(\mathbf{r}) + E_x^{s*}(\mathbf{r})E_y^s(\mathbf{r})] + \frac{1}{2}|E_y^s(\mathbf{r})|^2 \\ |E_y^s(\mathbf{r})|^2 \\ \frac{1}{2}|E_x^s(\mathbf{r})|^2 - \frac{1}{2}[E_x^s(\mathbf{r})E_y^{s*}(\mathbf{r}) + E_x^{s*}(\mathbf{r})E_y^s(\mathbf{r})] + \frac{1}{2}|E_y^s(\mathbf{r})|^2 \\ |E_x^s(\mathbf{r})|^2 + |E_y^s(\mathbf{r})|^2 \end{bmatrix}. \quad (8)
 \end{aligned}$$

Assuming that the speckle follows Gaussian statistics, the cross-covariance of the intensity at the observation plane in Fig. 1 becomes^[33-35]

$$\begin{aligned}
 C(\Delta\mathbf{r}) &= \langle \Delta I(\mathbf{r}) \cdot \Delta I(\mathbf{r} + \Delta\mathbf{r}) \rangle \\
 &= |\text{FT}\{I^t(\mathbf{r}_1, \theta)\} + \text{FT}\{I^R(\mathbf{r}_1, \theta)\}|^2, \quad (9)
 \end{aligned}$$

where $\Delta I(\mathbf{r}) = I(\mathbf{r}) - \langle I(\mathbf{r}) \rangle$ is the fluctuation of intensity with respect to its mean value. $\text{FT}\{I^s(\mathbf{r}_1, \theta)\} = W^s(\Delta\mathbf{r}, \theta) = \langle E^s(\mathbf{r}, \theta) \cdot E^{s*}(\mathbf{r} + \Delta\mathbf{r}, \theta) \rangle$ is the complex coherence function, where $\langle \rangle$ represents the spatial average as a replacement of the ensemble average, and FT is the 2D Fourier transform. It is important to note that an FT is used in Eq. (9), rather than an Fr (Fresnel transform), despite Fresnel propagation from the source to the observation plane at a distance z . Both sources (target and reference) are at distance z from the observation plane, and this helps to remove common curvature in the cross-covariance and generates a lensless Fourier transform geometry for the coherence waves^[35]. Therefore, we use a Fourier kernel (rather than Fresnel) in Eq. (9).

For a spatially fluctuating random field and under consideration of spatial ergodicity, the complex coherence, based on spatial averaging, is connected with the source at the scattering plane as follows^[33]:

$$W^t(\Delta\mathbf{r}, \theta) = \int I^t(\mathbf{r}_1, \theta) \cdot \exp\left(-i\frac{2\pi}{\lambda z} \Delta\mathbf{r} \cdot \mathbf{r}_1\right) d\mathbf{r}_1, \quad (10a)$$

$$W^R(\Delta\mathbf{r}, \theta) = \int \text{circ}\left(\frac{\mathbf{r}_1 - \mathbf{r}_g}{a}\right) \cdot \exp\left(-i\frac{2\pi}{\lambda z} \Delta\mathbf{r} \cdot \mathbf{r}_1\right) d\mathbf{r}_1, \quad (10b)$$

where the circ function represents a circular aperture function. \mathbf{r}_g is the off-axis position of the circular source, and a is the radius of the source. W^R provides a constant reference wave with carrier frequency to cover the support of W^t .

The Fourier transform of Eq. (9) produces the following terms:

$$\begin{aligned}
 \text{FT}\{C(\Delta\mathbf{r})\} &= I^t(\mathbf{r}_1, \theta) \otimes I^{t*}(\mathbf{r}_1, \theta) + I^R(\mathbf{r}_1, \theta) \otimes I^{R*}(\mathbf{r}_1, \theta) \\
 &+ I^t(\mathbf{r}_1, \theta) \otimes I^{R*}(\mathbf{r}_1, \theta) + I^{t*}(\mathbf{r}_1, \theta) \otimes I^R(\mathbf{r}_1, \theta), \quad (11)
 \end{aligned}$$

where \otimes is the 2D convolution operator. $I^t(\mathbf{r}_1, \theta)$ is the intensity of the target source at the scattering plane, and the intensity of the reference source $I^R(\mathbf{r}_1, \theta)$ is the off-axis circular function. The first two terms of Eq. (11) are auto-correlations, which provide a central direct-current (DC) component term. However, the last two terms are cross correlations and provide two laterally shifted copies, depending on \mathbf{r}_g .

In this study, the x component of the light from target $E_x^t(\mathbf{r}_1)$ carries the vortex information, and the y component $E_y^t(\mathbf{r}_1)$ is represented by a uniform distribution beam with a circular aperture. Here, the phase of the vortex beam can be simplified and expressed as $e^{il\phi_1}$, where l is the topological charge, and ϕ_1 is the azimuthal angle at the transverse plane. The two orthogonal components located at the source plane are mixed into the light, and the polarization and spatial modulation are entangled. A beam, with spatially varying polarization states due to OAM and orthogonal bases^[36], can be represented as $E^t(\mathbf{r}_1) = \hat{e}_x e^{il\phi_1} + \hat{e}_y E_y^t(\mathbf{r}_1)$.

However, if we consider the light from the reference as a -45° linearly polarized off-axis source, the two orthogonal components are $E_x^R(\mathbf{r}_1) = -E_y^R(\mathbf{r}_1) = \text{circ}[(\mathbf{r}_1 - \mathbf{r}_g)/a]$. Here, the radius a is small enough to provide a quasi-point source.

The resultant intensity expressions of the two sources, corresponding to different polarizer angles θ in Eq. (8), can be written as Eq. (12). In Eq. (12), Fr represents the propagation of light from the scattering plane to the observation plane. The intensity in Eq. (12) is a speckle, and it includes the contribution of the vortex and non-vortex information; however, the vortex information cannot be directly attained. The cross-covariance of the resultant speckle, relating to the intensity correlation, is calculated by the ensemble average of the intensity fluctuation, which helps to wash out the random phase introduced by the diffuser. Reconstruction results depend on the statistics not on the individual diffuser. According to the theoretical analysis, two important features about the diffuser need to be satisfied to assure the feasibility of proposed method. One is that the speckle field follows Gaussian statistics, and the other one is that the light does not depolarize when it transmits through the diffuser.

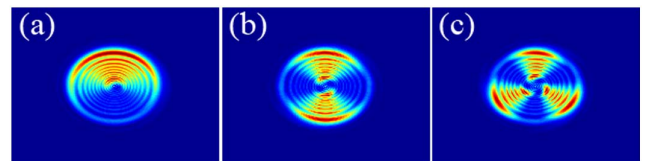


Fig. 2. Simulations of intensity pattern prior to the diffuser when the polarizer orientation is 45° . The topological charges of the vortex beams are 1, 2, and 3, respectively.

$$\begin{bmatrix} I(\mathbf{r}, 0^\circ) \\ I(\mathbf{r}, 45^\circ) \\ I(\mathbf{r}, 90^\circ) \\ I(\mathbf{r}, -45^\circ) \\ I(\mathbf{r}) \end{bmatrix} = \begin{bmatrix} |\text{Fr}[E_x^t(\mathbf{r}_1)]|^2 + |\text{Fr}[\text{circ}(\frac{r_1-r_x}{a})]|^2 \\ \frac{1}{2}|\text{Fr}[E_x^t(\mathbf{r}_1)]|^2 + \frac{1}{2}\{\text{Fr}[E_x^t(\mathbf{r}_1)] + \text{Fr}[E_x^{t*}(\mathbf{r}_1)]\} \cdot \text{Fr}[E_y^t(\mathbf{r}_1)] + \frac{1}{2}|\text{Fr}[E_y^t(\mathbf{r}_1)]|^2 \\ |\text{Fr}[E_y^t(\mathbf{r}_1)]|^2 + |\text{Fr}[\text{circ}(\frac{r_1-r_x}{a})]|^2 \\ \frac{1}{2}|\text{Fr}[E_x^t(\mathbf{r}_1)]|^2 - \frac{1}{2}\{\text{Fr}[E_x^t(\mathbf{r}_1)] + \text{Fr}[E_x^{t*}(\mathbf{r}_1)]\} \cdot \text{Fr}[E_y^t(\mathbf{r}_1)] + \frac{1}{2}|\text{Fr}[E_y^t(\mathbf{r}_1)]|^2 + 2|\text{Fr}[\text{circ}(\frac{r_1-r_x}{a})]|^2 \\ |\text{Fr}[E_x^t(\mathbf{r}_1)]|^2 + |\text{Fr}[E_y^t(\mathbf{r}_1)]|^2 + 2|\text{Fr}[\text{circ}(\frac{r_1-r_x}{a})]|^2 \end{bmatrix}. \quad (12)$$

Equation (12) represents the intensity, calculated by Eqs. (6) and (8) at the observation plane, with a polarizer oriented at a specific angle or without a polarizer. The intensity prior to the diffuser can be obtained by calculating the cross-covariance and subsequently performing the Fourier transform, as in Eq. (11). As illustrated in Fig. 2, the intensity distribution is obtained by propagating the orthogonal polarization components from the source plane to the random scattering plane using the angular spectrum method (ASM).

3. Experiment

To realize the scheme of Fig. 1, we design a compact setup, shown in Fig. 3. Two independent random diffusers are implemented for the target and reference sources by using two different portions of a common diffuser ground glass (GG, DG05-220, Thorlabs, 2 mm thickness). A horizontally polarized He-Ne laser is spatially filtered using a microscope objective (MO) and a pinhole (P), and collimated using a lens (L_1) of focal length of 150 mm. The collimated beam is converted into 45° linearly polarized with respect to the horizontal direction by a half-wave plate (HWP) and is then split into two arms by a beam splitter (BS). The reflected beam from the BS propagates towards the mirror (M) and generates a reference beam, which propagates towards the diffuser through the BS. The transmitted beam from the BS illuminates a reflective-type spatial light modulator (SLM). The SLM provides modulation in the horizontal direction and is used to impose a helical phase into one of the orthogonal components of light, leaving the other component intact. This arrangement provides a method to produce coaxial propagation of the orthogonal components of the light, from the SLM to the GG. To increase the size of the vortex core, the SLM

is slightly shifted from the focal plane of L_2 . The light from the SLM, which encodes target information, is then reflected by the BS and imaged at the GG plane, using a lens combination of L_2 and L_3 . The GG is positioned at the back focal plane of L_3 , and the focal lengths of L_2 and L_3 are both 300 mm. The reference beam provides an off-axis point source on the GG plane. The object beam and reference beam illuminate the GG at different positions, indicating that their speckles are statistically independent. The light from mirror M has a flipped polarization of -45° at the GG. The spot sizes of the light propagated from the SLM and M are different, owing to their geometrical arrangement, as shown in Fig. 3. The size of the spot from M is reduced, owing to the focusing of L_3 , and is positioned off-axis by tilting M. The speckle generated behind the GG is recorded by the CCD camera. Experiments were done for the vortex beam with topological charges from 1 to 3.

4. Experiment and Simulation Results

To compare our results with those of the simulation, we follow a two-pronged simulation strategy. In the first simulation, we simulate the complex field and intensity distribution prior to the diffuser. Here, we use the ASM to incorporate defocusing from the focal plane of L_2 to the SLM. The defocused field is expressed as $E_x^t(\mathbf{r}_1) = \text{IFT}\{\text{FT}\{e^{i\ell\phi}\} \times e^{i\frac{2\pi}{\lambda}z_0\sqrt{1-(\lambda\xi)^2-(\lambda\eta)^2}}\}$, where $\text{FT}\{\}$ and $\text{IFT}\{\}$ denote the Fourier transform and inverse Fourier transform, respectively. ξ and η are the spatial coordinates in the Fourier plane. z_0 refers to the defocusing distance, from the front focal plane of L_2 to the SLM plane. For the y component, the vortex term is replaced by a circular aperture in ASM. This simulation provides the intensity distribution prior to the diffuser, as shown in Fig. 2. In the second simulation strategy, we digitally propagate the complex field through the diffuser by incorporating a random phase. A random intensity is obtained using a suitable propagation kernel, as in Eq. (12). This intensity distribution is substituted in the cross-covariance relation in Eqs. (9) and (11), and the recovered intensity distributions from the simulated speckle patterns are obtained.

The Fourier transform of the cross-covariance for the vortex beam with topological charge 1 is shown in Fig. 4. The DC term in the center is suppressed to highlight the two conjugate spectra. The simulation results are performed by the second simulation strategy. The Fourier spectra produce two conjugated dark cores at off-axis locations for the polarizer rotation angle of 0° , as

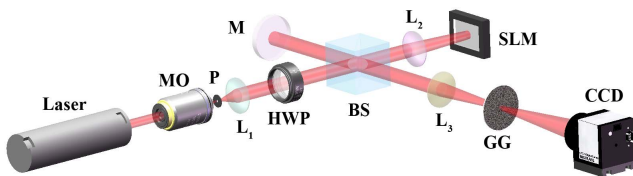


Fig. 3. Experimental setup for measuring the topological charge of the vortex beams from laser speckle. Laser, He-Ne laser; MO, microscope objective; P, pinhole; L_1 , L_2 , and L_3 , lens; HWP, half-wave plate; BS, beam splitter; M, mirror; SLM, spatial light modulator; GG, ground glass; CCD, charge coupled device.

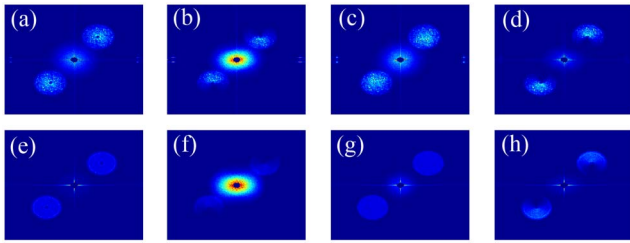


Fig. 4. Experimental results and numerical simulations of the Fourier transform of the cross-covariance for the vortex beam with topological charge 1. (a)–(d) are the experimental results for rotation angles of polarizer 0°, 45°, 90°, and –45°. (e)–(h) are the simulations corresponding to (a)–(d), respectively.

in Fig. 4(a). Comparing Fig. 4(a) with Fig. 4(e), the experimental results and numerical simulations are consistent.

Figure 4(b) presents the result for a polarizer orientation of 45°. The Fourier spectrum of the cross-covariance shows a lobe pattern, and the number of lobes is the same as the topological charge. This structure resembles the deterministic intensity structure, shown in Fig. 2(a). It should be noted that the intensity shown in Fig. 2(a) is calculated from the propagation of light from the source plane to the scattering plane, which can be considered as the theoretical prediction. Therefore, it is evident that we can retrieve the intensity in front of the diffuser from a non-imaged detected speckle pattern.

For a polarizer oriented at an angle of 90°, the Fourier spectrum is a uniform structure, shown in Fig. 4(c), because this polarization direction is orthogonal to the modulation direction of the SLM. Therefore, the vortex information is not available from the Fourier transform of the cross-covariance.

The Fourier transform of the cross-covariance for the –45° case (orientation along the polarization direction of light from the mirror) is similar to the 45° case. This is also primarily due to the contribution of the terms $|E_x^t(\mathbf{r})|^2$ and $E_x^t(\mathbf{r}) + E_x^{t*}(\mathbf{r})$. The orientation of the off-axis lobes in Fig. 4(d) is reversed, compared with Fig. 4(b), in accordance with the opposite signs of the second term in the intensity expressions for the 45° and –45° orientations.

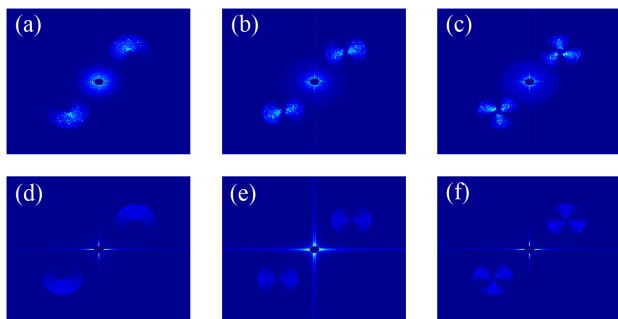


Fig. 5. Experimental results and numerical simulations of the Fourier transform of the cross-covariance for vortex beam case without a polarizer. (a)–(c) are the experimental results for topological charges 1, 2, and 3. (d)–(f) are the simulations corresponding to (a)–(c), respectively.

For the case of the absence of a polarizer before the detector, the Fourier spectrum results of the experiment and simulation are shown in Fig. 5. Because the intensity from the SLM is weaker than that from the mirror, the Fourier spectra in Fig. 5(a) are approximately the same as that for the –45° case in Fig. 4(d). The magnitude of the topological charge of a vortex beam can be obtained from the speckle by counting the number of lobes from the Fourier transforms of the cross-covariance. This is similar to the conventional method, which measures the topological charge of vortex beams by counting the number of interference patterns. However, it is noticeable that the conventional method requires a well-defined spiral phase, which is impractical in the case of a random diffuser. In particular, this novel method to measure the topological charge from the laser speckle requires only a single-shot measurement of intensity. Therefore, it can also be applied to a dynamic diffuser.

5. Conclusion

In this study, we measured the topological charge of vortex beams located behind a diffuser. This technique is based on the propagation property of the vortex beam and the cross-covariance of the intensity from the single-shot non-imaged resultant speckle pattern. We utilized the correlation properties of the speckle field, formed by the vortex beam propagating through a diffuser. Fourier spectra of the correlation function provide the signature of the topological charge of the propagating vortex beam. The results showed that the number of lobes generated by the Fourier spectra of the cross-covariance function is equal to the topological charge of the vortex beam, for cases of polarized states of $\pm 45^\circ$ and without a polarizer. The validity of the proposed technique is tested by both experiment and simulation.

Acknowledgement

This work was supported by the National Natural Science Foundation of China (NSFC) (No. 11674111), Fujian Province Science Funds for Distinguished Young Scholar (No. 2018J06017), Fundamental Research Funds for the Central Universities (No. ZQN-PY209), and Science and Engineering Research Board (SERB) (No. India-EMR/2015/001613).

References

- G. Gibson, J. Courtial, M. J. Padgett, M. Vasnetsov, V. Pas'ko, S. M. Barnett, and S. Franke-Arnold, "Free-space information transfer using light beams carrying orbital angular momentum," *Opt. Express* **12**, 5448 (2004).
- L. Gong, Q. Zhao, H. Zhang, X. Hu, K. Huang, J. Yang, and Y. Li, "Optical orbital-angular-momentum-multiplexed data transmission under high scattering," *Light: Sci. Appl.* **8**, 27 (2019).
- Z. Liu, S. Yan, H. Liu, and X. Chen, "Superhigh-resolution recognition of optical vortex modes assisted by a deep-learning method," *Phys. Rev. Lett.* **123**, 183902 (2019).

4. J. Wang, J. Yang, I. M. Fazal, N. Ahmed, Y. Yan, H. Huang, Y. Ren, Y. Yue, S. Dolinar, and M. Tur, "Terabit free-space data transmission employing orbital angular momentum multiplexing," *Nat. Photon.* **6**, 488 (2012).
5. S. Fu, Y. Zhai, H. Zhou, J. Zhang, C. Yin, and C. Gao, "Demonstration of high-dimensional free-space data coding/decoding through multi-ring optical vortices," *Chin. Opt. Lett.* **17**, 080602 (2019).
6. A. E. Willner, H. Huang, Y. Yan, Y. Ren, N. Ahmed, G. Xie, C. Bao, L. Li, Y. Cao, and Z. Zhao, "Optical communications using orbital angular momentum beams," *Adv. Opt. Photon.* **7**, 66 (2015).
7. A. Chong, C. Wan, J. Chen, and Q. Zhan, "Generation of spatiotemporal optical vortices with controllable transverse orbital angular momentum," *Nat. Photon.* **14**, 350 (2020).
8. Z. Zhu, W. Gao, C. Mu, and H. Li, "Reversible orbital angular momentum photon-photon conversion," *Optica* **3**, 212 (2016).
9. D. G. Grier, "A revolution in optical manipulation," *Nature* **424**, 810 (2003).
10. Q. Zhao, M. Dong, Y. Bai, and Y. Yang, "Measuring high orbital angular momentum of vortex beams with an improved multipoint interferometer," *Photon. Res.* **8**, 745 (2020).
11. J. Ng, Z. Lin, and C. T. Chan, "Theory of optical trapping by an optical vortex beam," *Phys. Rev. Lett.* **104**, 103601 (2010).
12. X. Li, H. Ma, H. Zhang, M. Tang, H. Li, J. Tang, and Y. Wang, "Is it possible to enlarge the trapping range of optical tweezers via a single beam?" *Appl. Phys. Lett.* **114**, 081903 (2019).
13. C. N. Alexeyev, Y. A. Egorov, and A. V. Vol'yar, "Mutual transformations of fractional-order and integer-order optical vortices," *Phys. Rev. A* **96**, 063807 (2017).
14. V. V. Kotlyar, A. A. Kovalev, and A. P. Porfirev, "Astigmatic transforms of an optical vortex for measurement of its topological charge," *Appl. Opt.* **56**, 4095 (2017).
15. V. V. Kotlyar, A. A. Kovalev, and A. V. Vol'yar, "Topological charge of a linear combination of optical vortices: topological competition," *Opt. Express* **28**, 8266 (2020).
16. W. Zhang, Q. Qi, J. Zhou, and L. Chen, "Mimicking Faraday rotation to sort the orbital angular momentum of light," *Phys. Rev. Lett.* **112**, 153601 (2014).
17. D. P. Ghai, S. Vyas, P. Senthilkumaran, and R. S. Sirohi, "Detection of phase singularity using a lateral shear interferometer," *Opt. Lasers Eng.* **46**, 419 (2008).
18. H. I. Sztul and R. R. Alfano, "Double-slit interference with Laguerre-Gaussian beams," *Opt. Lett.* **31**, 999 (2006).
19. D. Deng, M. Lin, Y. Li, and H. Zhao, "Precision measurement of fractional orbital angular momentum," *Phys. Rev. Appl.* **12**, 014048 (2019).
20. J. M. Hickmann, E. J. S. Fonseca, W. C. Soares, and S. Chávez-Cerda, "Unveiling a truncated optical lattice associated with a triangular aperture using light's orbital angular momentum," *Phys. Rev. Lett.* **105**, 053904 (2010).
21. C. Guo, L. Lu, and H. Wang, "Characterizing topological charge of optical vortices by using an annular aperture," *Opt. Lett.* **34**, 3686 (2009).
22. S. Zheng and J. Wang, "Measuring orbital angular momentum (OAM) states of vortex beams with annular gratings," *Sci. Rep.* **7**, 40781 (2017).
23. P. Vaity, J. Banerji, and R. P. Singh, "Measuring the topological charge of an optical vortex by using a tilted convex lens," *Phys. Lett. A* **377**, 1154 (2013).
24. J. P. C. Narag and N. Hermosa, "Probing higher orbital angular momentum of Laguerre-Gaussian beams via diffraction through a translated single slit," *Phys. Rev. Appl.* **11**, 054025 (2019).
25. D. Shen and D. Zhao, "Measuring the topological charge of optical vortices with a twisting phase," *Opt. Lett.* **44**, 2334 (2019).
26. M. I. Akhlaghi and A. Dogariu, "Single-shot coherent noise suppression by spatial interferometric heterodyning," *Opt. Lett.* **42**, 2378 (2017).
27. G. R. Salla, C. Perumangattu, S. Prabhakar, A. Anwar, and R. P. Singh, "Recovering the vorticity of a light beam after scattering," *Appl. Phys. Lett.* **107**, 021104 (2015).
28. R. K. Singh, R. V. Vinu, and S. M. Anandraj, "Recovery of complex valued objects from two-point intensity correlation measurement," *Appl. Phys. Lett.* **104**, 111108 (2014).
29. A. Bianchetti, P. Etchepareborda, and A. Federico, "Determining the fractional topological charge shifting in perfect vortices from laser speckle," *Opt. Commun.* **441**, 74 (2019).
30. R. V. Vinu and R. K. Singh, "Determining helicity and topological structure of coherent vortex beam from laser speckle," *Appl. Phys. Lett.* **109**, 111108 (2016).
31. O. S. Magaña-Loaiza, M. Mirhosseini, R. M. Cross, S. M. H. Rafsanjani, and R. W. Boyd, "Hanbury Brown and Twiss interferometry with twisted light," *Sci. Adv.* **2**, e1501143 (2016).
32. R. Liu, F. Wang, D. Chen, Y. Wang, Y. Zhou, H. Gao, P. Zhang, and F. Li, "Measuring mode indices of a partially coherent vortex beam with Hanbury Brown and Twiss type experiment," *Appl. Phys. Lett.* **108**, 051107 (2016).
33. M. Takeda, W. Wang, D. N. Naik, and R. K. Singh, "Spatial statistical optics and spatial correlation holography: a review," *Opt. Rev.* **21**, 849 (2014).
34. J. W. Goodman, *Statistical Optics* (Wiley-Interscience, 2000).
35. L. Chen, R. K. Singh, Z. Chen, and J. Pu, "Phase shifting digital holography with the Hanbury Brown-Twiss approach," *Opt. Lett.* **45**, 212 (2020).
36. B. N. Simon, S. Simon, F. Gori, M. Santarsiero, R. Borghi, N. Mukunda, and R. Simon, "Nonquantum entanglement resolves a basic issue in polarization optics," *Phys. Rev. Lett.* **104**, 023901 (2010).